THE JOURNAL OF PHYSICAL CHEMISTRY C

Article

pubs.acs.org/JPCC

Probing the Reaction Dynamics of Thermite Nanolaminates

Garth C. Egan,[†] Edward J. Mily,[‡] Jon-Paul Maria,[‡] and Michael R. Zachariah*[,†]

[†]Department of Chemical and Biomolecular Engineering and Department of Chemistry and Biochemistry, University of Maryland, College Park, Maryland 20742, United States

[‡]Department of Materials Science and Engineering, North Carolina State University, Raleigh, North Carolina 27606, United States

Supporting Information

ABSTRACT: Al/CuO reactive nanolaminate ignition was studied using temperature jump (T-Jump) heating for rates greater than 10^5 K/s. Multilayer samples were sputter deposited onto thin platinum filaments in alternating layers of Al and CuO. The filaments were resistively heated in a time-of-flight mass spectrometer (ToF-MS), while ignition and reaction were observed with high-speed video. A total deposited thickness of 1800 nm was maintained for all samples, while the number of bilayers was varied from 1 to 12. Increasing this value decreased the diffusion distances and increased the amount of interfacial area across which reaction could occur, while keeping the overall energy of the system constant. From 2 to 6 bilayers, the ignition temperature decreased from 1250 to 670 K and the overall reactivity increased. Past 6 bilayers, the ignition temperature only decreased slightly and there was little impact on the overall reactivity. This behavior is consistent with a mass-transport model where the predominant diffusing species exhibits a low activation energy (50 kJ/mol). Ignition temperature, which depends upon bilayer thickness, is found to be a good predictor of flame speed.

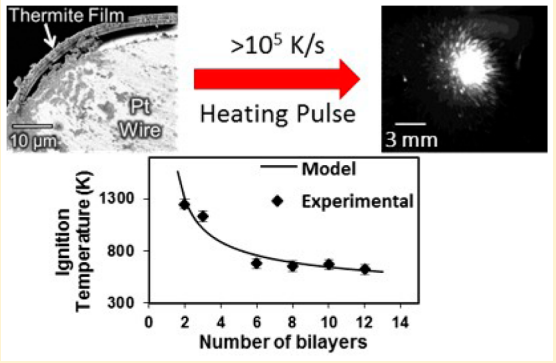

INTRODUCTION

Incorporating nanomaterials into thermite systems significantly improves the strongly exothermic oxygen exchange reaction between the metal fuel and metal oxide oxidizer. Nanoscale materials offer decreased diffusion distances and high interfacial surface area compared to traditional micron scale powders.[1−3] As a result, nanostructured thermite compositions have lower ignition temperatures and react faster, with flame speeds up to 1 km/s.[4] Most formulations involve nanoscale powders, but an alternative approach that offers great control of the resultant architecture is physical vapor deposition (PVD), in which alternating layers of fuel and oxidizer are stacked into planar structures, referred to commonly as reactive multilayers or nanolaminates.[5−8] Such structures are tunable and can be readily incorporated into MEMS processing, which makes them of interest for a variety of micropyrotechnic applications.[9,10] Regardless of the physical embodiment, much remains unknown about the processes and kinetics that control thermite ignition and reaction. Thus, the idealized form factor of nanolaminates provides a valuable avenue to explore this behavior. While reactive nanolaminates have been studied extensively at slower heating rates (~10 K/min) in differential scanning calorimetry or thermogravimetric experiments, complementary work is needed for heating regimes that more accurately reflect the combustion conditions that will exist during application.

In order to quantify the behavior of these materials under rapid heating, a temperature jump (T-Jump) technique (~10^5 K/s) was applied to Al−CuO reactive nanolaminates. This approach involves resistively heating thin platinum filaments that have been coated with the reactive multilayers. The ignition and reaction behavior of this material was observed with high-speed video and high temporal resolution time-of-flight mass spectrometry (ToF-MS). The total thickness and the fuel-oxidizer equivalence ratio (experimental fuel to oxidizer mass ratio divided by stoichiometric fuel to oxidizer mass ratio) of the samples were kept constant so that the total energy of reaction of each sample (assuming each goes to completion) was the same. The number of layers was varied from 1 bilayer (i.e., one pair of a fuel layer and an oxidizer layer) up to 12 bilayers. This allowed us to probe the influence of interface-to-volume ratio and the average diffusion distance on the reaction properties.

The simple planar geometry of these systems is ideal for understanding and modeling the kinetics of the diffusion processes that controls reaction. Because of this, we were able to fit a straightforward, diffusivity-based model for ignition to our results. Such models create a foundation for condensed phase thermite reactions, which is important to a wide range of thermite applications. For example, arrested reactive milled (ARM) materials are also dense and restricted to condensed phase reaction and recent work has shown that porous nanopowder thermites follow a condensed phase pathway as well.[11−15] While the exact nature of the interfaces can vary

Received: April 29, 2015
Revised: August 13, 2015
Published: August 13, 2015

DOI: 10.1021/acs.jpcc.5b04117
J. Phys. Chem. C 2015, 119, 20401−20408

between these materials, the results of this study may be applicable to a broader field than just the study of reactive nanolaminates.

EXPERIMENTAL SECTION

Sample Preparation. Nanolaminate layers were deposited onto a 76 μm diameter platinum filament using a dual magnetron sputtering chamber, previously described in another publication.[7] Multilayer films were fabricated by alternating the Al and CuO depositions allowing for 15 min between each deposition for the sputtering heat to dissipate. The sputter sources were 2″ in diameter oriented 180° from one another with shuttered confocal sources. The sputter targets (Al and CuO) were acquired from Kurt Lesker. The CuO target was indium bound to a copper backing plate to assist in heat dissipation during the sputtering. CuO was sputtered using an RF power supply with 100 W of power with a sputter pressure of 0.27 Pa of argon (purity > 99.9999%). Aluminum was sputtered using a DC power supply at 20 W of power with a sputter pressure of 0.4 Pa of argon. In order to prepare radially uniform thin multilayer thermite films, the Pt wire substrates were rotated on an axis perpendicular to the plane of the magnetron sputter guns at a rotation rate of 6 rpm. Prior to deposition, the wires were cleaned via 15 min of sonication in acetone and were then rinsed with deionized water, isopropyl alcohol, and methanol. They were mounted vertically and the center 10 mm of the wires were exposed to deposition where ∼5 mm of the wire ends were masked to allow for Pt electrical contact needed by T-Jump analysis. The laminate morphology and thickness were characterized by scanning electron microcopy (SEM) cross section analysis to obtain accurate deposition rates. The combination of small substrate diameter and rotation yielded deposition rates which were 40% lower in comparison to planar deposition on a flat surface. The deposition rates were 3.7 nm/min and 3.3 nm/min for Al and CuO respectively. Reference samples prepared on flat surfaces using identical deposition parameters were analyzed by X-ray photoelectron spectroscopy (XPS) to estimate copper valence. We routinely found that the Cu $2p_{3/2}$ peak was shifted from 932.4 to 933.6 eV, which is consistent with CuO. Furthermore, we found satellite peaks at 961, 941, and 943 eV which are only consistent with Cu in its 2+ valence. X-ray diffraction (XRD) on the wire deposited samples (1 and 12 bilayer) confirmed that the phases were consistent with planar samples and invariant to number of bilayers.

All samples were deposited starting with the metal layer first and all had a total thickness of 1800 nm. At each interface between Al and CuO a prereacted barrier forms (typically 2−4 nm).[16,17] So while the total thickness of each sample was the same, the samples with more interfaces featured more barrier material, which would decrease the overall energy of the system. However, the impact of this was ignored as even for the sample with the most bilayers (12), this accounted for only a 5% decrease. The fuel-oxidizer equivalence ratio was maintained at 1.4, which is fuel rich.

Characterization. The T-Jump/ToF-MS experimental set up was the primary means to investigate ignition, the details of which can be found in previous papers.[18−20] The nanolaminate coated Pt filaments were heated resistively with 3 ms DC electrical pulses to ∼1600 K. These pulses produced roughly linear heating rates of $\sim 4 \times 10^5$ K/s. The voltage and current measured from the wire were used to determine the time-resolved temperature based on the well-known relationship between Pt resistivity and temperature.[21] This temperature was correlated to the behavior observed simultaneously with a high speed camera (Phantom v12.0, 67 000 frames per second) and ToF-MS with spectra taken every 100 μs. The imaging allows for observation of visible combustion dynamics including overall optical intensity and ignition, which was considered as the first frame of sustained optical emission from the sample. After the first heating pulse and subsequent cooling, the wires were heated a second time to provide a background signal for video intensity and temperature.

Since Al deposited onto the platinum increases the net conductivity and the temperature is calculated from resistance, it is important to consider the impact of adding this initial layer. The cross-sectional area of a wire was 4.5×10^{-9} m^2, and the area of the thickest Al films (1 bilayer case) was 1.9×10^{-10} m^2, so the inclusion of the film represents only a 4% increase in area. But, given that the resistivity of Pt is ∼5 times higher than that of bulk Al, this can decrease the overall resistance by 12%, which is significant, although the grain structure of the thin films may increase the resistivity and lessen the impact of this effect. Regardless, no ignition measurement was made for 1 bilayer (as will be discussed below), and the potential impact of this effect decreases to 6%, 4%, and 2% for the 2, 3, and 6 bilayers, respectively. Additionally this effect can be measured experimentally, with a comparison of the temperature of the experimental heating pulses and background pulses. The continuity and morphology of the Al layer would be destroyed by the experimental heating, so any effect on resistance would be removed for the background run. Thus, if the diminished resistance from Al was significant, the experimental temperature reading at the start of the heating pulse would be lower than the background case. This effect was noticed in the 1 bilayer case (∼35 K difference in starting temperatures) and to a smaller degree in the 3 bilayer case (∼15 K difference), but not in any of the other cases. As we did not use any temperature data from the 1 bilayer case, and the difference in 3 bilayers was small relative to experimental variation, we ignored this effect.

RESULTS

A set of cross-sectional SEM images for the Al/CuO nanolaminate samples typical of this study is shown in Figure 1. The cross sections, prepared by cutting a coated wire with scissors, reveal microstructures with a columnar appearance and coarse interface roughness. The roughness and degree of columnarity in the present samples is larger than is typical of Al/CuO films prepared on semiconductor substrates like Si.[5,8] Microstructures in the present samples have a coarsened morphology as result of the wire surfaces, which are orders of magnitude rougher than a Si substrate, and from the fact that some fraction of the deposition occurs off-axis (i.e., deposition occurs on the sides and back side of the wire, but at a much slower rate than the leading surface). The kinetic energy of the species that deposit off-axis is lower and does not benefit from the additional atom mobility afforded by mild bombardment. The combination of these two effects produces this course grain morphology. Irrespective, the films are dense and continuous. It should also be noted that the delamination visible in Figure 1a and d occurred during the cross sectioning process. Film further back from the cross sectioned edge was well adhered to the Pt substrate as in Figure 1b and c.

For every sample, except the 1 bilayer nanolaminates, a clearly visible ignition and reaction could be observed from the high speed video. Figure 2 shows some frames taken from the

DOI: 10.1021/acs.jpcc.5b04117
J. Phys. Chem. C 2015, 119, 20401−20408

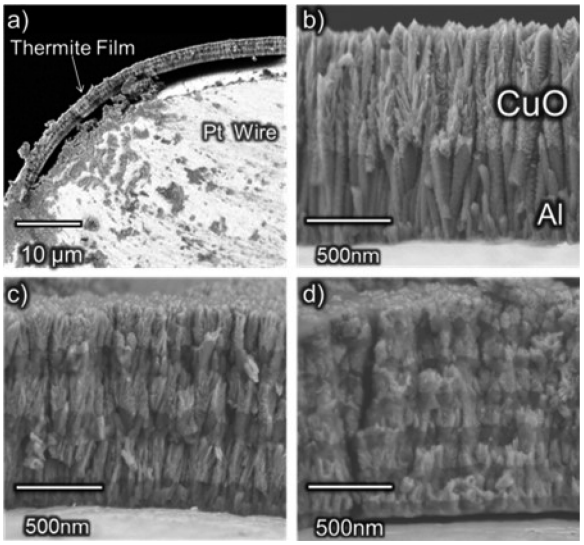

Figure 1. SEM image of Al/CuO nanolaminates coated Pt wires that were cleaved to show a cross section. Panel (a) shows the curvature of the films as deposited. The visible deformation of the wire is a result of the cross-sectioning process. Higher magnification images of 1, 3, and 6 bilayer samples are shown in panels (b), (c), and (d), respectively. All samples were deposited Al first and with CuO as the outermost layer.

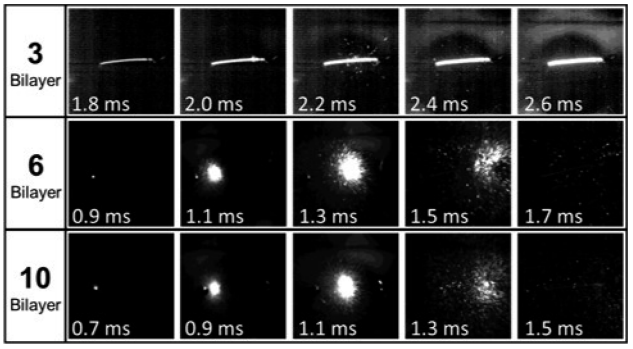

Figure 2. Frames from the high speed video of samples with 3, 6, and 10 bilayers. The brightness and contrast of the images for the 3 bilayer sample were digitally enhanced to make the reaction more visible. Frames shown were taken 0.2 ms apart and with 14 μs exposure time. The same scale was used for all images, with the bright wire in the 3 bilayer case being ~10 mm long.

high-speed video of experiments performed on 3, 6, and 10 bilayer samples. Each sample was subjected to a similar heating pulse, which means that the times indicated for each frame are proportional to the temperature of the wire at that instant. As can be seen, the 3 bilayer sample only reacted very weakly and at high temperatures. Comparatively, both the 6 and 10 bilayer samples reacted far more violently and at significantly lower temperatures. Based on these observations, the samples could be grouped into two categories: weak and violent. The weak group was made up of the 1, 2, and 3 bilayer samples and was characterized by minimal emission and ejection of material from the wire. The violent group contained the 6, 8, 10, and 12 bilayer sample, which all rapidly ejected large amounts of hot material from the wire surface as shown in Figure 2.

The point of ignition is shown in the first frames for both the 6 and 10 bilayer samples in Figure 2. By correlating the time of this frame with the temperature data of the wire, the ignition temperature can be determined. For 2, 3, and 6 bilayers, the ignition temperatures (±50 K) were 1250, 1130, and 680 K, respectively. The 8, 10, and 12 bilayer samples ignited at lower temperatures of 650, 670, and 620 K, respectively. There is a general trend of decreasing ignition temperatures with increasing number of bilayers that appears to saturate for samples that have high interfacial area to volume ratios. As the total thickness of all samples was constant, the number of bilayers is inversely proportional to bilayer thickness, which has been found to be a controlling property for nanolaminate reaction.[16,22,23] In those terms, the weakly reactive 1, 2, and 3 bilayer samples had bilayer thicknesses of 1800, 900, and 600 nm, respectively, while the violently reactive 6–12 bilayer samples had thicknesses of 300–150 nm. Thus, the comparative change in bilayer thickness was much less significant from 6 to 12 bilayers, which could help explain the similar reactivity in the violent group and diminishing change in ignition temperature.

In order to better quantify the reactivity, the integrated intensity of each frame of the high speed videos was determined. This data was normalized by the peak intensity of the background run taken with a second pulse of each wire. Examples of this data as plotted temporally are shown in Figure 3. It should be noted that that there was some run-to-run variation in the shape and size of the peaks, but the ones shown are representative of the general trends observed. As mentioned previously, for 1 bilayer, there was no ignition, which is reflected by the lack of any peaks in the intensity plot that are distinct from the background heating. Instead the signal has the same general shape as the background but slightly brighter. The increased brightness implies that some degree of exothermic reaction did occur, which led to a hotter wire. This was also reflected in the temperature profiles for these runs. The intensity profiles of 2 and 3 bilayer samples were similar to the 1 bilayer sample except with their ignition reflected by the small but distinct peaks prior to the end of the 3 ms heating pulse. They also reach higher peak intensities, suggesting more reaction occurring faster.

The transition between the weak group and the violent group is apparent with the extreme jump in reactivity from 3 to 6 bilayers. Rather than the peak intensity coinciding with the end of the heating pulse, the samples with more bilayers had emission occurring prior to 2 ms that was 5–10 times larger than the background. One interesting feature of these plots is

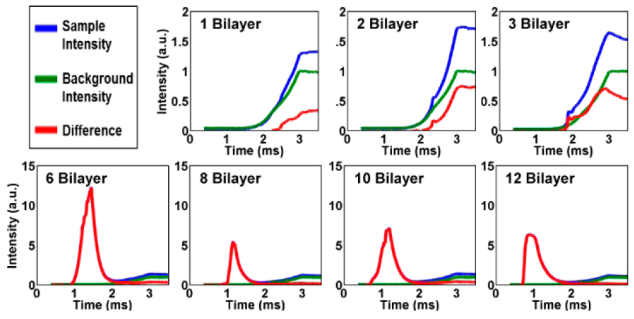

Figure 3. Integrated intensity taken from the frames of the high speed videos. Note the difference in scales between the two rows. The blue lines represent the heating and reaction of each sample, the green line represents a second run of the same wire, and the red line represents the difference between those two results. All data is normalized by the peak of the background run.

DOI: 10.1021/acs.jpcc.5b04117
J. Phys. Chem. C 2015, 119, 20401–20408

that the 6 bilayer samples featured the highest intensity, even though one might expect that the samples with the most bilayers would be the brightest and most reactive. Closer inspection of the images in Figure 2 reveals that while the 6 and 10 bilayer samples look similar, the visible material ejected from the 6 bilayer sample is coarser than that ejected by the 10 bilayer sample. Because of the camera settings, many of the pixels at the center of reaction were fully saturated. This means that the material thrown off the wire makes a disproportionate contribution to the integrated intensity measurement. Additionally, with finite camera resolution, finer bright material can get lost and larger bright material will contribute more to the overall intensity. As such, caution must be exercised when interpreting absolute intensity trends.

The transition in reactivity from weak to violent is also apparent in the mass spectra taken with the ToF-MS. Figure 4 shows the signal intensity of several species, along with the temperature of the wire for 3 and 6 bilayer sample runs. The mass spectra for the weak group (1−3 bilayer) were all qualitatively similar to the 3 bilayer case shown in Figure 1a, with a major O_2 peak, whose onset (defined as 5% of maximum) occurred at 1050 (±50) K and preceded ignition (vertical dashed line). Samples that ignited prior to this O_2 release threshold (6−12 bilayer samples), showed no or much less significant O_2 signals, which implies that the oxygen reacted with aluminum instead of being released to the chamber. It is likely that the oxygen signal observed for low bilayer samples resulted from the decomposition of the outermost layer of CuO ($2CuO \rightarrow Cu_2O + 1/2O_2$). Such behavior has been observed to occur at 975 K in CuO nanoparticles under similar heating conditions, and is consistent with the relative stabilities of CuO and Cu_2O at high temperatures and low pressures.[19] Another significant feature of the low bilayer mass spectrum is the lack of significant peaks for the species that normally indicate reaction (e.g., Cu, Al_2O, AlO).[18,20] While Figure 4a does show some intensity for m/z = 27 (labeled Al), there are organic compounds with that m/z (e.g., HCN, C_2H_3) that are more likely to be responsible, as there were significant C, H, and N species detected at that same time (e.g., m/z = 2, 12, 28, 44). The reason for this was likely surface contamination that occurred during handling.

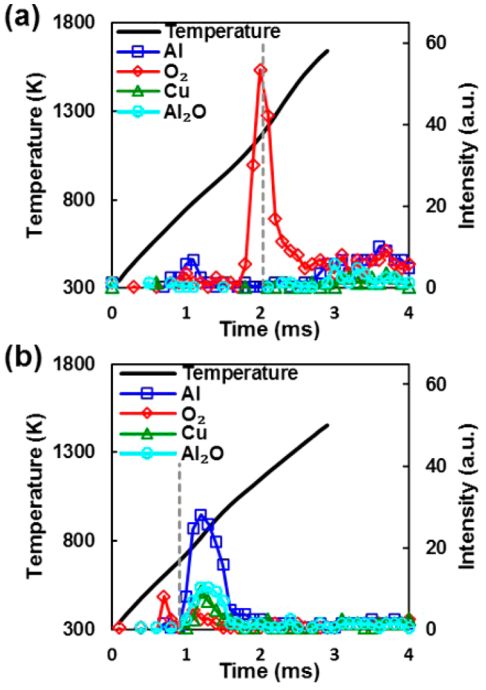

Figure 4. TOF-MS results from experiments for samples with (a) 3 bilayers and (b) 6 bilayers. The vertical dashed line indicates the time of ignition as determined from high-speed video.

In comparison, the violent samples all showed spectra similar to the 6 bilayer case shown in Figure 4b. These samples featured only minimal O_2 but had significant amounts of Al, Cu, and Al_2O. The onset of these peaks coincided with visible ignition observed with the high-speed camera. Since all the peaks shared the same profile, we can reasonably assume that all these species were the supposed reaction products rather than organic contamination discussed above. For all samples with 6 or more bilayers, Al is the most significant vapor phase reaction species, which may at first seem unusual considering that CuO was the terminal layer in each case. However, at similar temperatures, the equilibrium vapor pressure of Al is about twice that of Cu. Combining this information with the observation of violent delamination upon ignition of these more reactive samples (see Figure 2) leads to a self-consistent understanding that upon ignition most of the multilayer material is ejected from the wire surface and the "history" of the initial layering sequence is lost. Thus, the high temperature properties of the constituent elements predominate the experiment.

In order to better understand the material being ejected, product collection was performed in a manner similar to that found in a previous paper.[12] A carbon tape substrate was positioned ∼3 mm from the Pt filament, which was then heated at $\sim 10^5$ K/s. The product was analyzed using scanning electron microscopy (SEM) as is shown in Figure 5 for a 10 bilayer sample. Figure 5a shows the general product morphology, which are roughly spherical particles with average diameter of ∼4 μm. Figure 5b shows a higher magnification of the product using backscattered electrons (BSE), which cause the heavier elements (Cu) to show up brighter. Energy dispersive X-ray spectroscopy (EDS) was used to confirm that the bright phase was copper and the darker phase was oxidized aluminum. The near spherical shape of the product particles indicate they are formed in a molten state, which is to be expected given that the adiabatic flame temperature for this system (∼2800 K) is much higher than the melting point of Al_2O_3 (2345 K).[24] Also visible in this image, decorating the surface of the larger particle, are small nanoparticles (<50 nm) that were likely formed from

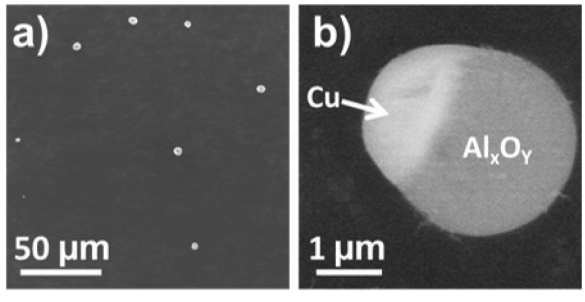

Figure 5. SEM images of product collected ∼3 mm away from a 10 bilayer sample. Panel (a) gives a view of the general morphology of the product. Panel (b) is an image of a single product particle taken using backscattered electrons (BSE), which show heavier elements (Cu) as brighter.

DOI: 10.1021/acs.jpcc.5b04117
J. Phys. Chem. C 2015, 119, 20401−20408

vapor phase condensation.[12] This experiment was also performed on the 3 bilayer case, which showed the same characteristic morphologies but with far less material collected due to the less violent reaction.

DISCUSSION

A primary benefit realized when studying reactive nanolaminates is that their geometrically simple embodiment facilitates studying and understanding the processes that controls reaction. Further since they are dense, reaction can only occur through condensed phase diffusion. With these features in mind, we developed a model based on 1D diffusion for nanolaminate ignition. We focus only on the reaction leading up to the point of ignition, because as discussed above the violence of the ignition process destroys the morphology and changes the amount of interfacial area.

For this model, we assume a planar geometry as the thickness of the film (1.8 μm) is small compared to the diameter of the wire substrate (76 μm). We also assume that the entirety of the nanolaminate is isothermal with the wires. This is reasonable because there is good interfacial contact between the layers and the wire. Using the reported thermal diffusivities of Al and CuO (8.3×10^{-5} and 5.1×10^{-6} m^2/s), a 1800 nm thick layer will have a characteristic time to thermal equilibrium (defines as length scale squared divided by the diffusivity) of ~40 and 640 ns for Al and CuO respectively.[25] This is much faster than the 3 ms heating time scale of the wire. We also assume that reaction is controlled by a diffusivity with Arrhenius behavior. This model focuses on the interfacial reaction that occurs leading up to the point of ignition, which is only a small portion of the overall reaction. Because of this we can neglect the oxygen loss that occurred prior to ignition in the 2 and 3 bilayer cases and the effect that the loss could have on the overall energy release of reaction. Any oxygen loss should occur from the surfaces open to the environment, which are farther than 100 nm from the reaction interfaces and thus should not affect the local interfacial oxygen concentration during the short time scale leading to ignition. Therefore, we can treat all samples the same despite the differences in reactivity discussed above.

From this basic framework we can model the change in temperature with the following three equations:

$$\frac{dT}{dt} = \frac{1}{C_p}\dot{Q}_{rxn} \tag{1}$$

$$\dot{Q}_{rxn} = nA\Delta H_{rxn}J \tag{2}$$

$$J = \nabla c D_0\, e^{(-E_a/RT)} \tag{3}$$

Equation 1 relates the temporal change in temperature to the rate of heat generation by reaction ($\dot{Q}_{rxn}$) divided by the heat capacity (C_p). The heat generated is evaluated in eq 2, where n is the number of interfaces, A (m^2) is the surface area of each interface, ΔH_{rxn} (J/mol) is the energy released from each mol of reaction, and J (mol/(s·m^2)) is the flux of oxygen through each interface. The interfacial area, A, can be calculated based on a cylinder with the diameter of the wire to be 2.4×10^6 m^2 for a 10 mm long film. The number of interfaces is related to the number of bilayers (N) through $n = 2N - 1$. While heat capacity is temperature dependent, the change is relatively small over the range of ignition temperatures determined here. For simplicity, the value at the average ignition temperature (830 K) was used for all cases. Equation 3 is the Fickian diffusion flux through each interface, where ∇c (mol/m^4) is the concentration gradient across the interface, D_0 is the pre-exponential to the diffusivity, and E_a is its activation energy. The concentration gradient is based on O anions going from zero to the concentration in CuO over the length of a typical interfacial Al_xO_y barrier layer ($\Delta x_b \sim 4$ nm) to be 2.0×10^{13} mol/m^4.[16]

The process of achieving ignition is not well-defined, but in these experiments ignition was observed as localized, very rapid increases in brightness that occurred discontinuously from the wire heating. As such, ignition marks a decoupling of wire and film temperatures, with the film temperature rapidly increasing above that of the wire. For this reason, we chose to define ignition temperature (T_{ign}) as the point at which the temperature rise from reaction (eq 1) exceeds the heating rate from the wire (5×10^5 K/s). Combining eqs 1−3 and solving for ignition temperature gives

$$T_{ign} = -\frac{E_a}{R}\left(\ln\left(\frac{(5 \times 10^5\ \text{K/s})C_p}{n\nabla c\Delta H_{rxn}AD_0}\right)\right)^{-1} \tag{4}$$

Apart from the two variables that define diffusivity (D_0 and E_a), all other constants are well-defined or can be reasonably estimated. Diffusivity is not as well-known, because there is a wide range in the available data, and it is unclear which species is the primary diffusant. Therefore, the fit to the experimental data used D_0 and E_a as tunable parameters. Additionally, all these values are temperature independent, except for concentration gradient (∇c), which would change as the barrier layer (Δx_b) grows from reaction with $\nabla c(T) = \Delta c/\Delta x_b(T)$. The growth of the barrier layer is determined by the flux of oxygen ions, which thickens the Al_2O_3 side of the barrier and depletes oxygen from the CuO side. Therefore, the change in barrier thickness can be written as

$$\frac{d\Delta x_b}{dt} = J(3V_m^{Al_2O_3} + V_m^{CuO}) \tag{5}$$

Here, $V_m^{Al_2O_3}$ and V_m^{CuO} are the molar volumes (m^3/mol) of Al_2O_3 and CuO, respectively, and J (mol/(s·m^2)) is the flux as given in eq 3. From this, with a known D_0 and E_a, the barrier layer thickness can be modeled by numerically integrating with the constant heating rate. However, as we are starting with unknown values of D_0 and E_a, we employed an iterative model refinement approach to determining these parameters. To start, a constant concentration gradient was assumed and eq 4 was fit to the experimental data, giving the values E_a = 20 kJ/mol and $D_0 = 9.0 \times 10^{-13}$ m^2/s. Then the barrier layer growth was determined by numerically integrating eq 5 with these parameters. Then a new fit was made based on a modified independent variable ($n\nabla c$) that combined the experimental number of bilayers with the concentration gradient predicted by the model for that value of n. This generated a new set of D_0 and E_a that was used to start the next iteration. This process was continued until convergence, when the values for E_a and D_0 remained constant through further iterations. More details on this procedure can be found in the Supporting Information.

The modeled ignition temperature is shown with the experimental data in Figure 6a. The black solid line is the fit made from the assumption of a constant concentration gradient (E_a = 20 kJ/mol, $D_0 = 9.0 \times 10^{-13}$ m^2/s), and the dashed gray line is the result of the iterative refinement (E_a = 49 kJ/mol, $D_0 = 2.9 \times 10^{-10}$ m^2/s) that takes into account the barrier layer

DOI: 10.1021/acs.jpcc.5b04117
J. Phys. Chem. C 2015, 119, 20401−20408

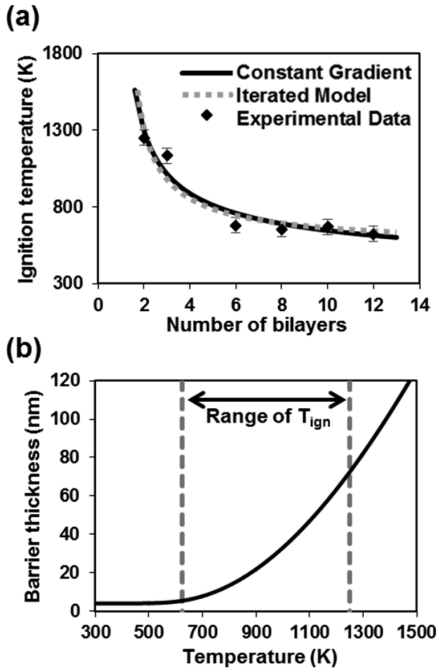

Figure 6. Results from the iteratively refined model. Panel (a) shows the modeled ignition temperature with number of bilayers assuming a constant concentration gradient and from the refined model that included a dynamic gradient. Panel (b) shows the expected barrier layer growth determined from the numerical integration of eq 5 *and* used in the iterated model fit shown in panel (a).

growth shown in Figure 6b. The barrier growth can be seen to be rather insignificant at the point of the lower ignition temperatures (~6 nm total thickness) but quite large by the upper end of the ignition range (~70 nm). The refined fit is slightly worse (R^2 coefficient of 0.91 vs 0.94) than the other, but given the significant barrier accumulation over this range of ignition temperatures, it is a better representation of the physical process.

Figure 7 illustrates the sensitivity of this model to activation energy. The dashed and dotted lines represent the best fits that can be achieved (using the iterative refinement and oxide growth) when restricting E_a to 100 and 200 kJ/mol, respectively. Assuming a higher activation energy results in energy release becoming far more sensitive to temperature,

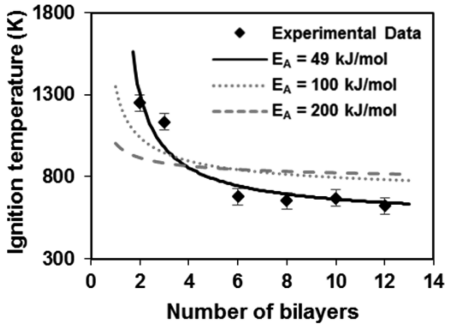

Figure 7. Experimentally determined ignition temperatures plotted with iteratively refined modeling results. The solid black line is the best fit model to the experimental data (E_a = 49 kJ/mol, $D_0 = 2.9 \times 10^{-10}$ m^2/s). The dotted and dashed lines shown are model results with activation energies of 100 and 200 kJ/mol, respectively, using $D_0 = 1.2 \times 10^{-7}$ and 1.3×10^{-1} m^2/s.

which in turn decreases the sensitivity to the number of bilayers. This effect is clearly seen in Figure 7 (dashed line) for E_a = 200 kJ/mol, where ignition temperature is relatively flat, meaning it is only weakly dependent on number of bilayers. With this in mind it is surprising that the value for E_a found here is so low, because the controlling process to ignition is presumably diffusion through the Al_2O_3 layer that forms between components during deposition.[6,7,16] While there is a wide range of values for the various diffusion mechanisms in Al_2O_3, activation energies are typically 200−600 kJ/mol.[26] However, most data on diffusivity in alumina is for the α phase, while the barrier layer that forms in nanolaminates is amorphous.[6,7,16] More recent results have shown a lower activation energy (116 kJ/mol) for that diffusion of oxygen ions in amorphous Al_2O_3, but even that is still significantly higher than the value found here.[27] Previous results have shown that high heating rates can lead to a reduction in activation energy, although the exact origins of this low activation energy remains to be determined and will be a focus of further study.[28]

Regardless of how this occurs, these results imply that, at the high heating rates, condensed phase kinetics can be faster than what would be expected from reference diffusivity values. This could help explain some of the confusion over nanoparticle thermite combustion, where low diffusivities have been used to rule out certain modes of combustion.[29] These reactive nanolaminate results suggest that a condensed phase mechanism is fast enough to be responsible for the reactivity observed in nanoparticle thermites, given sufficient interfacial surface area. Both systems being driven by the same mechanism is further supported by the similarity between the product morphology shown in Figure 5 and that collected from Al/CuO nanoparticle reaction.[12]

As a final point, we work to understand the implications of our results in terms of applications more general than uniform heating. In particular, we want to relate this data to freely propagating combustion measurements of flame speed that are commonly used to gauge reactivity.[16,22,23] To do so, we consider flame propagation as essentially a series of sequential ignitions and neglect any reaction prior to that point. Given some length (Δx) of nanolaminate, the amount of energy needed to reach ignition is proportional to the ignition temperature (T_{ign}). In keeping with our previous discussion of ignition, we assume that it occurs when the segment of film reaches a critical reaction rate on a per mass basis, with the number of bilayers controlling the temperature at which that value is reached. Since this heat production at the point of ignition is bilayer independent, it is reasonable to assume that the heat flux forward into the cold film from that point is also constant, which implies a constant thermal gradient. Making this assumption, the time to reach ignition (Δt) will also be proportional to ignition temperature. This is represented schematically in the temperature versus time plot in Figure 8. The flame speed is the speed of the ignition front, which is then just ($\Delta x/\Delta t$).

Based on this approach, we calculate flame speed by taking the conductive heat flux and dividing it by the energy needed to reach ignition ($(W/m^2)/(J/m^3) \rightarrow m/s$). For simplicity we assume that the heat flux is independent of bilayer thickness and estimate it based on Fourier's Law. We use the thermal conductivity of Al (240 W/mK) and base the constant thermal gradient on a temperature rise from 300 to 650 K (the lower bound ignition temperatures) over a distance of 1 μm (chosen to fit data). The energy needed to reach ignition, is based on

DOI: 10.1021/acs.jpcc.5b04117
J. Phys. Chem. C 2015, 119, 20401−20408

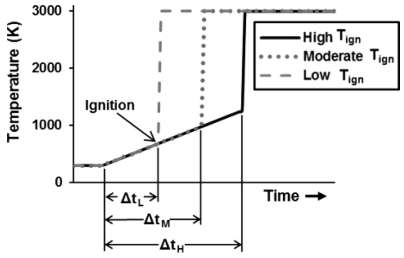

Figure 8. Schematic representation of the temperature profiles of some segment (Δx) of reactive foil as the flame front moves across it. The different lines represent the effect of different ignition temperatures on the time scale of ignition. Δt_L, Δt_M, and Δt_H are the time needed for a foil segment to reach a low, moderate, and high ignition temperature, respectively.

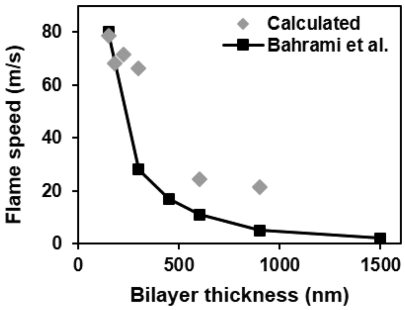

Figure 9. Flame speeds as calculated from the experimentally determined ignition temperatures. Also shown are experimental flame speed results as reported by Bahrami et al.[16]

the change in standard enthalpy of formation from room temperature to the ignition point. The results of these calculations are plotted in Figure 9 along with flame speed data for sputter deposited Al/CuO nanolaminates reported by Bahrami et al.[16] The values calculated here from ignition temperature show the same trend as the experimentally determined values. This suggests the flame speed, ignition temperature, and bilayer thickness can all be directly correlated to one another. As the amount of interfacial area per unit mass increases, ignition temperature falls while flame speed rises rapidly. This trend occurs because thinner bilayers have less mass per reacting interface, which promotes faster self-heating at lower temperatures. Further, the agreement shown in Figure 9 reflects that the heating rates used in these experiments ($\sim 10^5$ K/s) sufficiently reproduce the kinetics of combustion.

CONCLUSIONS

Al/CuO reactive nanolaminates of a constant thickness but varied number of bilayers were sputter deposited onto Pt filaments. These filaments were heated at $\sim 4 \times 10^5$ K/s and the reactivity was characterized with high speed video and ToF-MS. Increasing the number of bilayers, and thus deceasing bilayer thickness, was found to enhance reactivity and lower ignition temperature. For samples with fewer than 3 bilayers, only O_2 and no other species expected from reaction were detected with mass spectroscopy. In comparison, the strongest signals for samples with 6 or greater bilayers were Al, Al_2O, and Cu. A simple diffusion based model was developed and fit to the experimentally determined ignition temperatures. From this model, it was determined that a low activation energy (50 kJ/mol) was likely controlling the ignition process. With similar analysis, the experimentally determined ignition temperatures were used to calculate flames speeds. The results of these calculations were found to be in good agreement with experimentally determined values.

ASSOCIATED CONTENT

Supporting Information

The Supporting Information is available free of charge on the ACS Publications website at DOI: 10.1021/acs.jpcc.5b04117.

Details of the iterative refinement of the model (PDF)

AUTHOR INFORMATION

Corresponding Author

*E-mail: mrz@umd.edu.

Notes

The authors declare no competing financial interest.

ACKNOWLEDGMENTS

Work conducted by M.R.Z and G.C.E. has been supported by the Army Research Office (Ralph Anthenien) and the Defense Threat Reduction Agency. J.-P.M. and E.J.M. acknowledge Ralph Anthenien and the U.S. Army Research Office for financial support under contract W911NF1310493. We acknowledge the support of the Maryland NanoCenter and its AIMLab.

REFERENCES

(1) Dreizin, E. L. Metal-based Reactive Nanomaterials. *Prog. Energy Combust. Sci.* **2009**, *35*, 141−167.

(2) Rogachev, A. S.; Mukasyan, A. S. Combustion of Heterogeneous Nanostructural Systems (Review). *Combust., Explos. Shock Waves* **2010**, *46*, 243−266.

(3) Yetter, R. A.; Risha, G. A.; Son, S. F. Metal Particle Combustion and Nanotechnology. *Proc. Combust. Inst.* **2009**, *32*, 1819−1838.

(4) Weismiller, M. R.; Malchi, J. Y.; Lee, J. G.; Yetter, R. A.; Foley, T. J. Effects of Fuel and Oxidizer Particle Dimensions on the Propagation of Aluminum Containing Thermites. *Proc. Combust. Inst.* **2011**, *33*, 1989−1996.

(5) Blobaum, K. J.; Reiss, M. E.; Plitzko, J. M.; Weihs, T. P. Deposition and Characterization of a Self-Propagating CuOx/Al Thermite Reaction in a Multilayer Foil Geometry. *J. Appl. Phys.* **2003**, *94*, 2915−2922.

(6) Petrantoni, M.; Rossi, C.; Salvagnac, L.; Conedera, V.; Esteve, A.; Tenailleau, C.; Alphonse, P.; Chabal, Y. J. Multilayered Al/CuO Thermite Formation by Reactive Magnetron Sputtering: Nano Versus Micro. *J. Appl. Phys.* **2010**, *108*, 084323.

(7) Kwon, J.; Ducere, J. M.; Alphonse, P.; Bahrami, M.; Petrantoni, M.; Veyan, J.-F.; Tenailleau, C.; Esteve, A.; Rossi, C.; Chabal, Y. J. Interfacial Chemistry in Al/CuO Reactive Nanomaterial and Its Role in Exothermic Reaction. *ACS Appl. Mater. Interfaces* **2013**, *5*, 605−613.

(8) Mily, E. J.; Oni, A.; LeBeau, J. M.; Liu, Y.; Brown-Shaklee, H. J.; Ihlefeld, J. F.; Maria, J. P. The Role of Terminal Oxide Structure and Properties in Nanothermite Reactions. *Thin Solid Films* **2014**, *562*, 405−410.

(9) Rossi, C.; Esteve, D. Micropyrotechnics, a New Technology for Making Energetic Microsystems: Review and Prospective - Review. *Sens. Actuators, A* **2005**, *120*, 297−310.

(10) Rossi, C.; Esteve, A.; Vashishta, P. Nanoscale Energetic Materials. *J. Phys. Chem. Solids* **2010**, *71*, 57−58.

(11) Egan, G. C.; LaGrange, T.; Zachariah, M. R. Time-Resolved Nanosecond Imaging of Nanoscale Condensed Phase Reaction. *J. Phys. Chem. C* **2015**, *119*, 2792−2797.

(12) Sullivan, K. T.; Piekiel, N. W.; Wu, C.; Chowdhury, S.; Kelly, S. T.; Hufnagel, T. C.; Fezzaa, K.; Zachariah, M. R. Reactive Sintering: An Important Component in the Combustion of Nanocomposite Thermites. *Combust. Flame* **2012**, *159*, 2−15.

DOI: 10.1021/acs.jpcc.5b04117
J. Phys. Chem. C 2015, 119, 20401−20408

(13) Stamatis, D.; Ermoline, A.; Dreizin, E. L. A Multi-Step Reaction Model for Ignition of Fully-Dense Al-CuO Nanocomposite Powders. *Combust. Theory Modell.* **2012**, *16*, 1011−1028.
(14) Schoenitz, M.; Ward, T. S.; Dreizin, E. L. Fully Dense Nano-Composite Energetic Powders Prepared by Arrested Reactive Milling. *Proc. Combust. Inst.* **2005**, *30*, 2071−2078.
(15) Jacob, R. J.; Jian, G.; Guerieri, P. M.; Zachariah, M. R. Energy Release Pathways in Nanothermites Follow Through the Condensed Phase. *Combust. Flame* **2015**, *162*, 258−264.
(16) Bahrami, M.; Taton, G.; Conedera, V.; Salvagnac, L.; Tenailleau, C.; Alphonse, P.; Rossi, C. Magnetron Sputtered Al-CuO Nano-laminates: Effect of Stoichiometry and Layers Thickness on Energy Release and Burning Rate. *Propellants, Explos., Pyrotech.* **2014**, *39*, 365−373.
(17) Mily, E. J. *Thermite at the Nano-Scale*. Ph.D. Thesis, North Carolina State University, May 2015.
(18) Jian, G.; Piekiel, N. W.; Zachariah, M. R. Time-Resolved Mass Spectrometry of Nano-Al and Nano-Al/CuO Thermite under Rapid Heating: A Mechanistic Study. *J. Phys. Chem. C* **2012**, *116*, 26881−26887.
(19) Zhou, L.; Piekiel, N.; Chowdhury, S.; Zachariah, M. R. Time-Resolved Mass Spectrometry of the Exothermic Reaction between Nanoaluminum and Metal Oxides: The Role of Oxygen Release. *J. Phys. Chem. C* **2010**, *114*, 14269−14275.
(20) Jian, G.; Chowdhury, S.; Sullivan, K.; Zachariah, M. R. Nanothermite Reactions: Is Gas Phase Oxygen Generation from the Oxygen Carrier an Essential Prerequisite to Ignition? *Combust. Flame* **2013**, *160*, 432−437.
(21) Childs, P. R. *Practical Temperature Measurement*; Butterworth-Heinemann: Woburn, MA, 2001.
(22) Alawieh, L.; Weihs, T. P.; Knio, O. M. A Generalized Reduced Model of Uniform and Self-Propagating Reactions in Reactive Nanolaminates. *Combust. Flame* **2013**, *160*, 1857−1869.
(23) Mann, A. B.; Gavens, A. J.; Reiss, M. E.; VanHeerden, D.; Bao, G.; Weihs, T. P. Modeling and Characterizing the Propagation Velocity of Exothermic Reactions in Multilayer Foils. *J. Appl. Phys.* **1997**, *82*, 1178−1188.
(24) Sullivan, K. T.; Kuntz, J. D.; Gash, A. E. The Role of Fuel Particle Size on Flame Propagation Velocity in Thermites with a Nanoscale Oxidizer. *Propellants, Explos., Pyrotech.* **2014**, *39*, 407−415.
(25) Edwards, A. L. *Compilation of Thermal Property Data for Computer Heat-Conduction Calculations*; California Univ., Livermore, Lawrence Radiation Lab: Livermore, CA, 1969.
(26) Heuer, A. H. Oxygen and Aluminum Diffusion in Alpha-Al2O3: How Much Do We Really Understand? *J. Eur. Ceram. Soc.* **2008**, *28*, 1495−1507.
(27) Nabatame, T.; Yasuda, T.; Nishizawa, M.; Ikeda, M.; Horikawa, T.; Toriumi, A. Comparative Studies on Oxygen Diffusion Coefficients for Amorphous and Gamma-Al2O3 Films Using O-18 Isotope. *Jpn. J. Appl. Phys., Part 1* **2003**, *42*, 7205−7208.
(28) Jian, G.; Zhou, L.; Piekiel, N. W.; Zachariah, M. R. Low Effective Activation Energies for Oxygen Release from Metal Oxides: Evidence for Mass-Transfer Limits at High Heating Rates. *ChemPhysChem* **2014**, *15*, 1666−1672.
(29) Levitas, V. I.; Pantoya, M. L.; Dikici, B. Melt Dispersion versus Diffusive Oxidation Mechanism for Aluminum Nanoparticles: Critical Experiments and Controlling Parameters. *Appl. Phys. Lett.* **2008**, *92*, 011921.

DOI: 10.1021/acs.jpcc.5b04117
J. Phys. Chem. C 2015, 119, 20401−20408